Chapter 21

In-Situ Tests on Liquefaction Potential of Subsoils

Grand entrance to the tomb of the third emperor of Tang Dynasty and his powerful empress, near Xi'an, China.

21.1 Use of SPT for Assessing Liquefaction Potential

The evaluation of F_L stated in Sect. 19.4 required laboratory tests on undisturbed soil specimens of loose sand. Undisturbed sampling of loose sand under the ground water table is not an easy job. The quality of samples might be poor unless an experienced engineer is engaged.

SPT-N is a measure of sand density. Meyerhof (1957) proposed an empirical correlation between N, σ'_v (effective vertical stress), and D_r (relative density in %);

$$D_r(\%) = 21\sqrt{\frac{N}{\sigma'_v\ (kgf/cm^2)+0.7}}\ . \qquad (21.1)$$

Since liquefaction resistance of loose to medium loose sand has been said to be proportional to D_r (Fig. 20.4), an SPT-based assessment of in-situ liquefaction resistance seems possible. Although relative density (D_r) and liquefaction resistance are essential characteristics of soil, SPT-N is not. This is because N value is affected by the effective stress (σ'_v); very loose sand may have high SPT-N under high stress level.

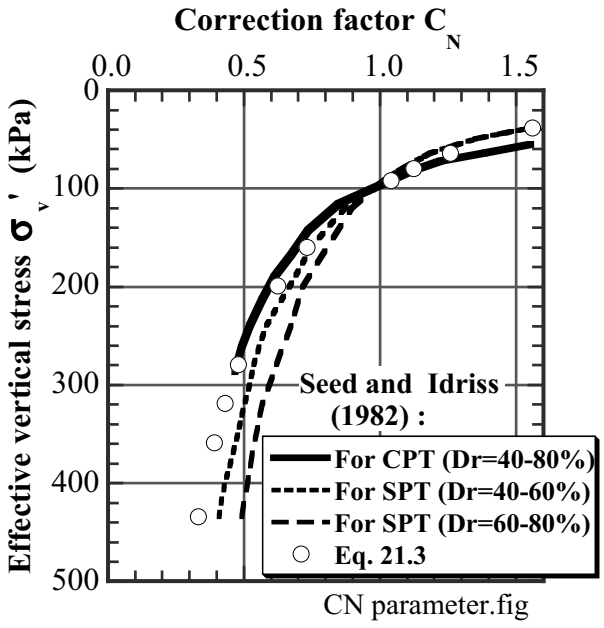

Fig. 21.1 Correction of SPT-N for effective stress level (Seed and Idriss, 1982)

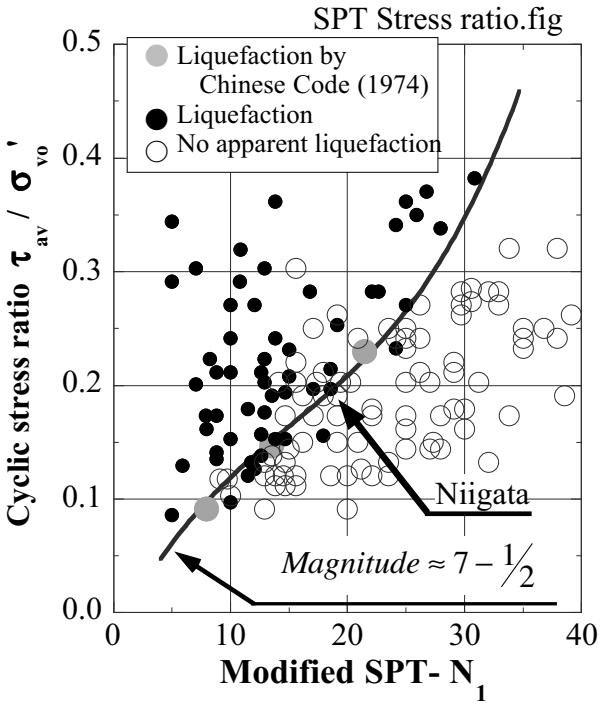

Fig. 21.2 Seismic stress ratio produced by earthquakes of magnitude = 7.5 at sites with and without liquefaction (Seed and Idriss, 1982)

Equation (21.1) suggests a way to correct SPT-N for the effects of stress level:

$$N_1 = C_N \times N\ , \qquad (21.2)$$

in which N_1 stands for the SPT-N at the effective stress level of 1 t/m^2 (98 kPa), and C_N designates a correction factor. Among many correction factors, (21.1) leads to

$$C_N = \frac{1.7}{\left[\sigma'_v(\text{kPa})/98\right]+0.7}. \qquad (21.3)$$

Seed and Idriss (2002) presented correction factors for both SPT (standard penetration tests) and CPT (cone penetration tests). Figure 21.1 compares those factors together with (21.3).

Seed and Idriss (1982) collected information about the earthquake-induced stress ratio and SPT-*N* at sites of past liquefaction and sites without liquefaction. It was then attempted to study the relationship between onset of liquefaction and SPT-*N*. To use the essential characteristics of sand, modified values of N_1 was employed in place of *N*. Although not being very precise, their results in Fig. 21.2 shows the boundary between data from liquefied and unliquefied sites, which infers the liquefaction resistance of sand and can be correlated with *N*. It should be noted that this diagram is valid for earthquake magnitude of 7.5 for which the number of cycles is about 15 (Table 19.1). The use of SPT-*N* for assessment of liquefaction resistance of soil (e.g., Sect. 21.4) is thus justified.

It is well known that fines content in sandy soil reduces the measured *N* value (Sect. 1.12). To account for this, there are several empirical corrections, and one of them is tabulated in Table 21.1. Another correction from the viewpoint of liquefaction is presented in Sect. 21.4.

Table 21.1 Correction of N_1 value of sandy soil in terms of fines content , F_c (Seed, 1987)

F_c (%)	ΔN
10	1
25	2
50	4
75	5

$$(N_1)_{effective} = (N_1)_{observed} + \Delta N$$

One of the early methods of assessment of liquefaction potential relied on SPT-*N* as well. Figure 21.3 was employed previously by the Code for Design of Oil and LNG Storage Tanks. Remedial measures against liquefaction was required when *N* was less than the critical value (N_{cr}) in this diagram. This early idea of N_{cr} came from the case studies in 1960s, which was conducted in Niigata city after extensive liquefaction (Sect. 21.2). As fines content (clay and silt, finer than 75 μm) increases in Fig. 21.3, N_{cr} decreases, because cohesive materials increase the liquefaction resistance and decreases the *N* value. Note that this early idea of critical *N* does not take into account the intensity of expected earthquakes and local earthquake activities. Actually, the seismic activity of Japanese Archipelago was intended by previous codes. Hence, the critical *N* value thus obtained is not valid in other parts of the world.

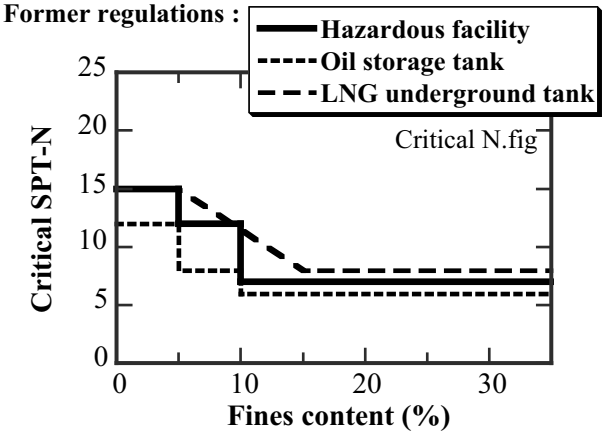

Fig. 21.3 Minimum SPT-*N* to resist against liquefaction in different codes

A similar assessment on liquefaction potential based on V_s does not yet work properly because V_s does not tell about type of soil (fines content).

21.2 SPT-*N* Observed in Niigata City

A great number of data were collected in Niigata City after the earthquake in 1964, making it possible to find a relationship between occurrence of liquefaction and SPT profile. Figure 21.4 shows a profile obtained before and after liquefaction. Liquefaction most probably occurred in layers where sand was densified and SPT-*N* value increased after the earthquake. This is due to densification after reconsolidation of liquefied loose sand. In contrast, SPT-*N* sometimes decreases after the quake probably due to dilatancy (volume expansion) of denser sand in consequence of shaking and disturbance. Hence, the boundary of the original *N* values that increased and decreased after the quake shows the largest *N* of liquefied sand. Koizumi (1966) presented this critical *N* as shown in Fig. 21.5. This finding led to a design criteria in Fig. 21.3. Figure 21.6 is a similar diagram on the critical *N* as a boundary of heavy and light damages in buildings.

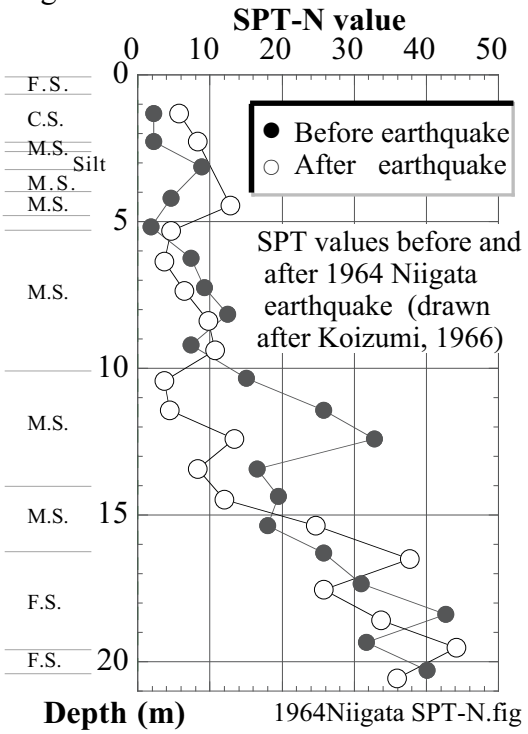

Fig. 21.4 SPT profile in Niigata before and after the earthquake (Koizumi 1966)

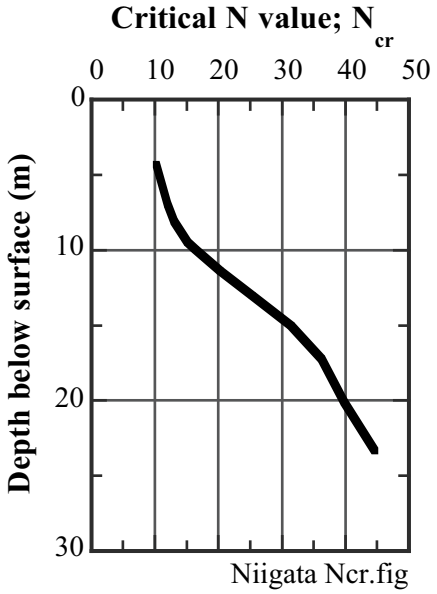

Fig. 21.5 Maximum *N* in liquefied layers of Niigata City (Koizumi, 1966)

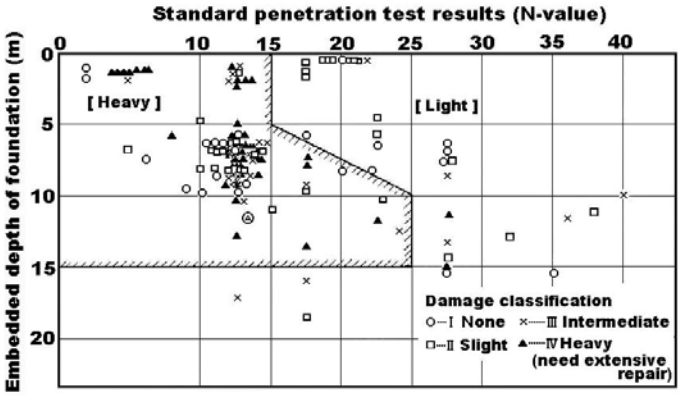

Fig. 21.6 Boundary line between light and heavy damage as related to *N* (Kishida, 1966)

21.3 Assessment of Liquefaction Potential

The risk of liquefaction of a specified site during a future earthquake has been assessed by one of the three approaches in what follows. Each of them has a different way to evaluate the magnitude of seismic load as well as the resistance of soil against liquefaction.

Table 21.2 Classification of practical assessments of liquefaction potential

Method	Seismic load	Resistance of soil	Concerned sections
1. Critical SPT-N	Out of scope	SPT-N < 15 for example is considered to mean high possibility of liquefaction	21.1 and 21.2
2. Factor of safety F_L=Resistance / Load	Shear stress amplitude = Surface acceleration (A_{max}) × (Mass of soil)	Obtained from cyclic undrained triaxial tests, or its empirical correlation with SPT-N and fines content	19.3 and 21.4
2′. Modification of 2.	Put in time history of earthquake. Dynamic analysis is run to obtain maximum seismic shear stress	Ditto	
	This is called total stress analysis		
3. Effective stress analysis	Put in time history of earthquake. Information on nonlinear stress–strain behavior of soil is needed	Parameters for negative-dilatancy model (pore water pressure model) are needed; laboratory tests on undisturbed samples	22.3 and 22.4
	Dynamic analysis is numerically run on the basis of the effective stress principle		

Notes:

– Method 1 was obtained from SPT-N values measured in Niigata city after the quake. Higher N values in sand mean greater density. This method is therefore meaningful to a certain extent. The problem is that the intensity of earthquake motion is out of scope. Regions of higher and lower seismic activities are treated equally, which is not a rational way. This method is being replaced by others in the recent times.

– The simplified calculation of load in Method 2 avoids dynamic analyses, which require additional soil investigations on V_s (shear wave velocity), G_{max}, and nonlinear stress-strain behavior.

– Recent developments of dynamic analysis technique have allowed the improvement of method from 2 to 2'. This analysis is called *Total Stress Analysis* in which the degradation of soil modulus and shear strength due to development of excess pore water pressure (decrease in effective stress) is not taken into account. In this sense, this analysis is not so sophisticated as effective stress analysis in 3.

– Substantial researches on dilatancy and constitutive models of sand produced the effective stress analysis in 3. Shear stress and strain at every moment of time is combined with the dilatancy model and change of excess pore water pressure as well as effective stress is calculated. The effective stress is then put in the stress–strain model to update the shear modulus and shear strength. This interaction of two models is carried out in every time increment of analysis. It is also possible to perform a seepage/consolidation analysis to obtain more reasonable effective stress. Today, the effective stress analysis is widely used in many important construction projects.

21.4 Assessment of Liquefaction Potential by SPT-*N* Before 1995

The method of critical SPT-*N* value shown in Sects. 21.1 and 21.2 was very simple. It pays attention only to soil condition, and ignores the intensity of seismic load. Hence, this method cannot calculate F_L value. Most codes today calculate the resistance against liquefaction, R, by using SPT-*N* and then compare it with the seismic stress ratio, L; $F_L = R/L$. An example is taken of Highway Bridge Design Code, which has been influencing many other codes. This section is going to present a previous version of this code because it is easy to understand, is good for education, and will be used in the exercise of this book. A more recent version will be described later in Sects. 21.7 and 21.8.

In the use of SPT-*N*, attention should be paid to possible errors or variation in practice in "standard" penetration procedure. Seed et al. (1985) mentioned the problems of insufficient impact energy, length of rod, and type of sampler (Sect. 1.12). Poor maintenance of the tip makes penetration more difficult. Noteworthy is that all these problems tend to increase the measured *N* value and consequently overestimate the soil strength.

In the Highway Bridge Design Code, liquefaction potential has to be examined when the ground water table is within 20 m from the surface and the mean grain size, D_{50}, is between 0.02 mm and 2.0 mm. No examination is required at depth more than 20 m, because soil at that depth is considered to be pleistocene or older, which is unlikely to liquefy.

It is recently recognized that such cohesionless fine materials as mine tailings 鉱滓 can liquefy (Sect. 20.5). Liquefaction of gravelly materials was discussed in Sect. 20.2 as well. Some extent of rise in excess pore water pressure at depth more than 20 m was reported in Port Island of Kobe, 1995. Hence, details of the code are subjected to change.

The resistance, R, consists of three components

$$R = R_1 + R_2 + R_3,$$

in which R_1 stands for the effects of density (Fig. 21.7)

$$R_1 = 0.0042 \times (\text{assessed relative density, \%})$$
$$= 0.0042 \times 21 \sqrt{\frac{N}{\sigma_v' \ (kgf/cm^2) + 0.7}}.$$

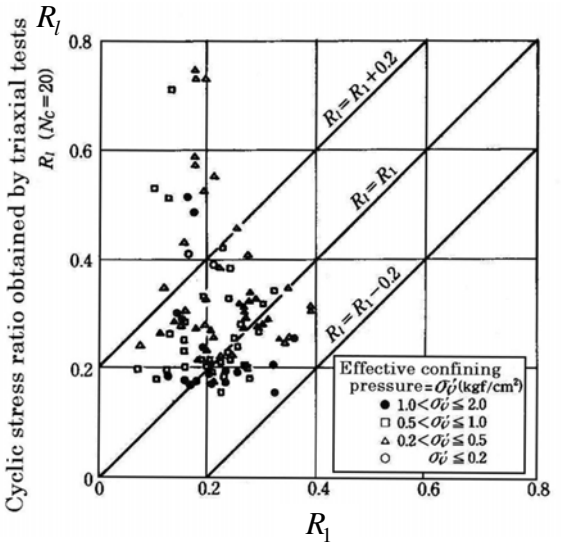

Fig. 21.7 Cyclic stress ratio obtained by triaxial tests and assessed relative density (Former version of Highway Bridge Design Code)

$R_2 = R_l - R_1$

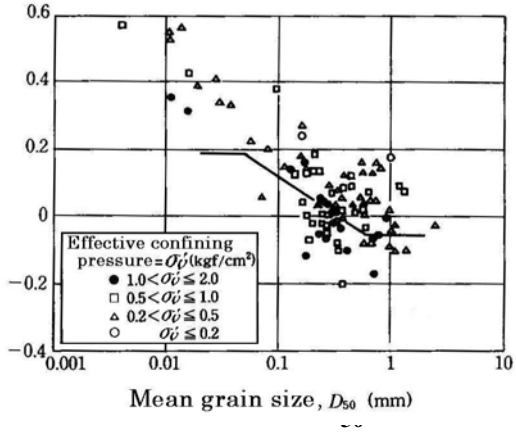

Fig. 21.8 Correction of stress ratio by means of mean grain size (Former version of Highway Bridge Design Code)

$R_3 = R_l - R_1 - R_2$

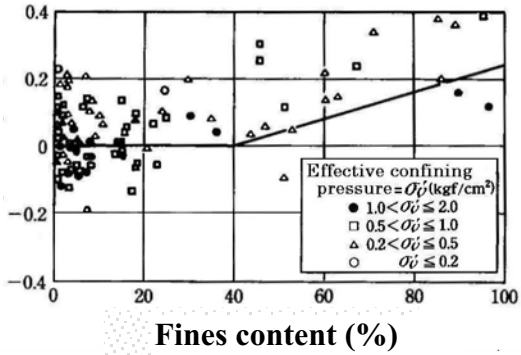

Fig. 21.9 Correction of stress ratio by means of fines content (Former version of Highway Bridge Design Code)

See (21.1). Since R_1 above cannot precisely give the experimentally measured liquefaction resistance, R_l, a correction was made by using the mean grain size, D_{50}. When the grain size is small, soil is supposed to be clayey and has an increased resistance against liquefaction (Sect. 20.4). In calculation, N of clayey soil tends to be smaller and R_1 may underestimate the resistance. Thus, the average curve in Fig. 21.8 was proposed for correction

$$\begin{aligned} R_2 &= 0.19 && \text{when} \quad 0.02\ \text{mm} \le \mathrm{D}_{50} \le 0.05\ \text{mm} \\ R_2 &= 0.225\log_{10}\left(0.35/D_{50}\right) && \text{when} \quad 0.05\ \text{mm} \le \mathrm{D}_{50} \le 0.6\ \text{mm} \\ R_2 &= -0.05 && \text{when} \quad 0.6\ \text{mm} \le \mathrm{D}_{50} \le 2.0\ \text{mm}. \end{aligned}$$

Since R_2 correction was found insufficient, a further correction has been made by R_3, which is based on fines content (F_C: silt and clay, finer than 75 μ) (see Fig. 21.4);

$$R_3 = 0.0 \text{ when } 0\% \le F_c \le 40\%, \text{ and } R_3 = 0.004\ F_c - 0.16 \text{ when } 40\% \le F_c \le 100\%.$$

In this code, r_d=1–0.015 × depth (in meter*)* is used for calculation of load (L) (Sect. 19.2). Consequently, the safety factor (resistance against liquefaction) is determined by

$$F_L = R/L.$$

21.5 Exercise No. 6: Calculation of Factor of Safety Against Liquefaction

This exercise employs the 1990 version of Highway Bridge Design Code. By learning this version, it becomes easy to understand the significance of its modification in 1995. Use $r_d = 1 - 0.015z$.

See Sect. 21.4 and calculate F_L by using the data as shown in the figure on the right and the table below:

Depth of ground water table =1.2 m
Unit weight of soil above water table = 1.4 tf/m^3
Unit weight of soil below water table = 1.9 tf/m^3
Design A_{max} at the surface = 0.15 G

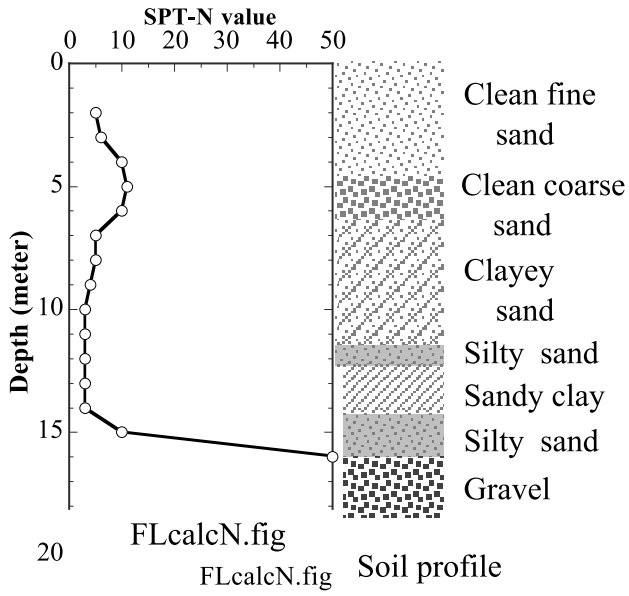

Depth (m)	SPT-N	Fines content F_c (%)	D_{50} (mm)	Type of soil
2	5	0.0	0.2	Clean fine sand
3	6	0.0	0.2	Ditto
4	10	0.0	0.3	Ditto
5	11	0.0	0.7	Clean coarse sand
6	10	0.0	0.7	Ditto
7	5	5.0	0.25	Clayey sand
8	5	5.0	0.25	Ditto
9	4	7.0	0.15	Ditto
10	3	10.0	0.15	Ditto
11	3	15.0	0.15	Ditto
12	3	41.0	0.06	Silty sand
13	3	80.0	0.02	Sandy clay
14	3	80.0	0.02	Ditto
15	10	5.0	0.4	Silty sand
16	50	1.0	2.0	Gravel

Remarks on ground water table: Evidently, the assessment of liquefaction risk is made of soils below the ground water table. The depth of ground water affects the effective stress in the subsoil. Thus, it is essentially important to determine precisely the elevation of ground water table, and many boring log (record) describes this information obtained from the water level in a bore hole. The problem is the uncertainty of the water table due to many reasons. For example, seasonal change is difficult to assess. Water leakage from a bore hole into gravelly layer may be significant. In an urban area, deep excavation of building foundation is often associated with pumping of ground water and lowering of the local water table. Hence, the judgment of water level should take into account the regional geological environment.

21.6 Issue for Future Development of Code

The existing code is never considered to be good enough. Experiences obtained in real earthquakes have been continuously demanding its revision and correction. The major issues of modification in recent times are as follows:

1. Dense sand
When SPT-*N* is large in dense sand, the true liquefaction resistance increases drastically (Fig. 20.4), whereas many existing codes assume a simple proportionality between resistance and relative density. The resistance is underestimated.

2. Equivalent number of loading cycles
Also, the equivalent number of cycles, equivalent to an irregular stress history, is assumed to be 20. Since the resistance is substantially larger at smaller number of loading cycles (Fig. 19.5), the resistance is underestimated when the number of cycles is small. In contrast, earthquakes of magnitude greater than 8 consist of a greater number of cycles.

3. Pleistocene soil
Being more than 10,000 years old, pleistocene sands have a high rigidity, a large SPT-*N* value, and consequently a sufficient resistance against liquefaction. Hence, its liquefaction has been considered unlikely. The 1995 Hyogoken Nambu earthquake, however, induced some extent of excess pore water pressure in a pleistocene layer at the bottom of Port Island. Hence, it was learned that an earthquake with a short distance from the source may induce heavy shaking and pore pressure increase even in a relatively stable pleistocene soil.

4. Sand with fines
Nonplastic fine soil is prone to liquefaction. When a loose fabric structure of coarser sand grains is associated with loose nonplastic fine powder, the potential of liquefaction is high. Since existing design codes pay less attention to nature of fines, whether plastic or nonplastic, the assessment of liquefaction potential is incomplete.

5. Design A_{max} at surface
A_{max} is the surface acceleration specified for design and had been conventionally assumed to be around 15% of gravity acceleration. Since A_{max} of as large as 340 Gal was recorded, however, at the ground surface of liquefied site in Port Island (Fig. 17.48), A_{max} was increased in codes and may be reviewed again in future. It should be taken into account that the number of cycles in the Port Island shaking was small (Figs. 17.47 and 17.48).

6. Use of numerical tools in determining the field stress ratio
It is evident that the rigid-column evaluation of stress ratio caused by an earthquake (19.1) is nothing but a rough approximation, although it is easy to use. A use of such analytical and numerical methods as an equivalent linear analysis and finite element procedures are being considered.

7. Subsoil investigation which is more reliable than SPT-*N*
Although being popular and of a large background database, SPT is relatively approximate and is a time consuming tool. Also, SPT is not reliable in gravelly subsoil. A possible use of cone penetration and shear wave measurement has been studied. Both these methods are quick and economical, not requiring drilling of a bore hole. The use of these method that do not collect soil specimen, however, seems difficult, unless it is combined with other methods, because loose liquefiable sand and medium-stiff unliquefiable clay can exhibit a similar value of V_s (Sect. 22.5). Many CPT of V_s correlation with liquefaction relies on conversion to SPT-*N* except the one by Shibata and Teparaksa (1988, Fig. 21.21).

21.7 Revised Design Prediction of Liquefaction After 1995: Part 1, Design Load

The lesson learned from liquefaction events during the 1995 Kobe earthquake was that liquefaction can be still fatal when the epicentral distance is very short (Sect. 5.10), the number of cycles is small, but the intensity of acceleration is substantial. After this earthquake, many design codes were revised and will be revised further in the near future. The revised code is described below by taking an example of the Highway Bridge Design Code.

1. Design earthquakes

Two kinds of design earthquakes are proposed; type I is the one that occurs in the tectonic subduction zone (Sect. 3.2) and has a greater earthquake magnitude; e.g., >7.5. With a longer duration time, the number of loading cycles is larger. In contrast, type II occurs inside a tectonic plate. Although its seismic magnitude is smaller and the duration time is shorter than those of type I, the short epicentral distance leads to a greater acceleration in an area of a limited size.

2. Soil conditions susceptible to liquefaction

Risk of liquefaction has to be studied for alluvial water-saturated sand when

- The sand lies within 20 m from the surface while the ground water table lies within 20 m from the surface,
- The fines content (<75 μ, silt and clay) is less than 35% or the plasticity index, I_p, is less than 15% (cohesion is small), and
- The mean grain size, D_{50}, is smaller than 10 mm while D_{10} < 1 mm (excluding gravel, although gravelly sand is included).

3. Judgement of liquefaction potential

The possibility of liquefaction is judged by using a kind of factor of safety; $F_L = R/L$, in which R and L stand for resistance and load, respectively.

Table 21.3 Classification of subsoil

Class I	$T_G < 0.2$ s	Hard
Class II	$0.2 \le T_G < 0.6$	
Class III	$0.6 \le T_G$	Soft

4. Load

A formula of $L = (1 - 0.015z)(\sigma_v / \sigma'_v)(c_z k_{hc0})$ gives the loaded stress ratio (Fig. 19.3). The depth from the surface (meter) is designated by z, while σ_v and σ'_v denote the total and effective vertical stresses. Moreover, $c_z k_{hc0}$ is the seismic coefficient for design as determined below

Table 21.4 Standard seismic coefficient

Subsoil class	Design earthquake	
	Type I	Type II
I	0.30	0.80
II	0.35	0.70
III	0.40	0.60

(a) Classify the surface soil layer by using the natural period, T_G

$$T_G = 4 \sum_{\text{layers}} \frac{\text{Layer thickness}}{V_s}. \quad (21.4)$$

This calculation is made of shallow clayey layers with SPT-N<25, sandy layers of N<50, or V_s<300 m/s. If in-situ V_s is not available, use formula in Sect. 8.4. For classification, see Table 21.3. Note that (21.4) is nothing more than an approximate calculation of the natural period.

(b) The standard seismic coefficient, k_{hc0}, is determined according to the subsoil classification and the type of design earthquake (Table 21.4).

The values in Table 21.4 is much greater than the conventional value of 0.15. The "c_z" parameter takes account of the regional seismic activity and ranges from 0.7 to 1.0. For example, c_z = 1 in Tokyo and Kanto area together with Osaka. Only Okinawa has the lowest value of c_z = 0.7.

21.8 Revised Design Prediction of Liquefaction After 1995: Part 2, Resistance Against Liquefaction

5. Resistance against liquefaction, *R*

The resistance stress ratio, *R*, is calculated as

$$R = C_{\mathrm{w}} R_{\mathrm{L}}, \tag{21.5}$$

in which R_{L} is the resistance as would be observed in cyclic undrained triaxial tests and C_{w} represents the effects of type of loading.

Although the triaxial resistance, R_{L}, should be determined by running laboratory tests on undisturbed good-quality specimens, this practice requires time-consuming and costly procedures. In most situations, therefore, R_{L} is determined by using SPT-*N*.

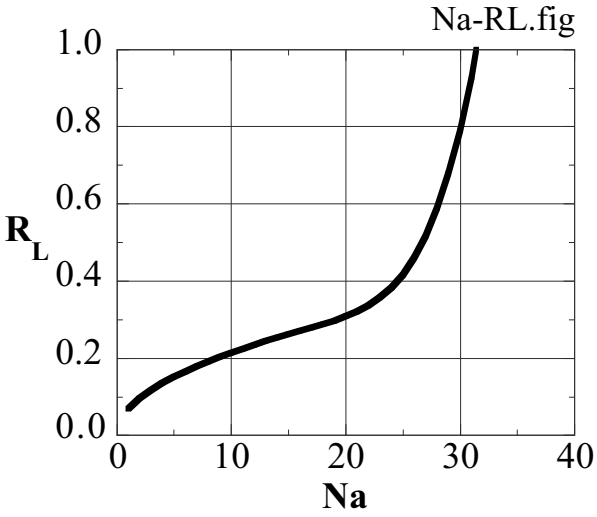

Fig. 21.10 Variation of design resistance of soil against liquefaction with SPT-N

(a) Adjusted *N* value, N_{a}

$$N_{\mathrm{a}} = c_1 \times \left(\frac{1.7N}{\sigma'_{\mathrm{v}} + 0.7} \right) + c_2 \qquad \text{for sand} \qquad \text{and}$$

$$N_{\mathrm{a}} = \left\{ 1 - 0.36 \ \log_{10}\left(\frac{D_{50}}{2} \right) \right\} N_1 \qquad \text{for gravelly soil} \tag{21.6}$$

where

$$c_1 = \begin{cases} 1 & \left(0\% \le F_{\mathrm{c}} < 10\%\right) \\ \left(F_{\mathrm{c}} + 40\right)/50 & \left(10\% \le F_{\mathrm{c}} < 60\%\right) \\ \left(F_{\mathrm{c}}/20\right) - 1 & \left(60\% \le F_{\mathrm{c}}\right) \end{cases} \quad \text{and} \quad c_2 = \begin{cases} 0 & \left(0\% \le F_{\mathrm{c}} < 10\%\right) \\ \left(F_{\mathrm{c}} - 10\right)/18 & \left(10\% \le F_{\mathrm{c}}\right) \end{cases},$$

where F_{c} stands for the fines content (finer than 75 μ). Note that $N_1 = \dfrac{1.7N}{\sigma'_{\mathrm{v}} + 0.7}$ removes the influence of the effective vertical stress level, σ'_{v} (kg/cm^2), from SPT-*N* value and gives the penetration resistance under $\sigma'_{\mathrm{v}} = 1\mathrm{kgf/cm}^2$ (=98 kN/m^2). Since $c_1 = 1$ and $c_2 = 0$ for F_{c} = 0% (clean sand), N_{a} is understood to be the SPT-*N* value for clear sand without fines.

(b) Determination of R_{L}

Two formulae are used in accordance with the quality and density of soil

$$R_{\mathrm{L}} = \begin{cases} 0.0882\sqrt{N_{\mathrm{a}}/1.7} & (N_{\mathrm{a}} < 14) \\ 0.882\sqrt{N_{\mathrm{a}}/1.7} + 1.6 \times 10^{-6}\left(N_{\mathrm{a}} - 14\right)^{4.5} & (14 \le N_{\mathrm{a}}) \end{cases} \tag{21.7}$$

The second formula above comes from the fact that dense sand of greater *N* has a liquefaction resistance dramatically greater than that of loose sand (Fig. 20.4). Figure 21.10 illustrates the variation of R_{L} with the increase in N_{a}. Note that this R_{L} is supposed implicitly to be the liquefaction resistance under 15–20 cycles of loading.

(c) Effects of type of loading

Conventionally, the irregular time history of earthquake loading has been converted to 20 uniform cycles of an equivalent amplitude by supposing a greater magnitude or type I earthquake. When the type II with

less number of cycles has to be taken into account from now on, the soil resistance against a smaller number of cycles should be employed. This goal is achieved by increasing the conventional strength by a factor of C_w. See that liquefaction resistance for less number of cycles is greater, in particular for dense sand (Fig. 20.2).

$$\text{For type I, } C_w = 1.0 \quad \text{and} \quad \text{for type II, } C_w = \begin{cases} 1.0 & \left(R_L \le 0.1\right) \\ 3.3R_L + 0.67 & \left(0.1 < R_L \le 0.4\right) \\ 2.0 & \left(0.4 < R_L\right) \end{cases} \tag{21.8}$$

Note that dense sand with greater R_L receives a larger value of C_w. It seems interesting that this new version of code does not use the mean grain size (D_{50} of fine soil) any more.

21.9 Factor of Safety Against Liquefaction and its Correlation With Extent of Damage

When the factor of safety against liquefaction, F_L, is less than 1.0, the concerned soil layer is considered to liquefy under the design earthquake condition. It is noteworthy, however, that this small F_L value in a limited soil layer does not mean the overall liquefaction-induced disaster at the surface.

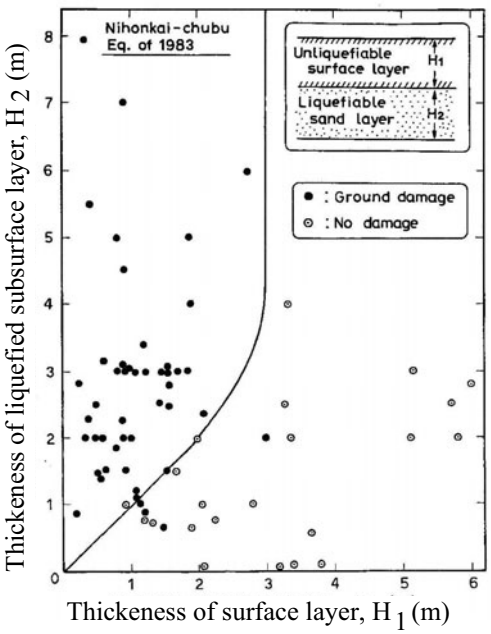

Fig. 21.11 Empirical relationship between thickness of liquefied and unliquefied layers with and without surface damage (Ishihara, 1985)

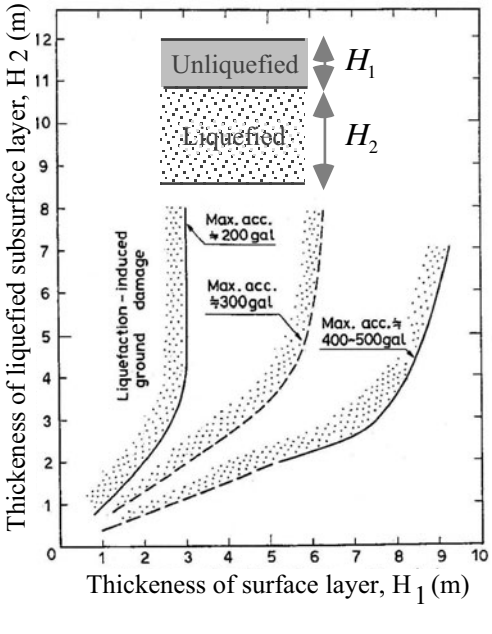

Fig. 21.12 Effects of thickness of unliquefied surfacelayer on mitigation of liquefaction-induced damage (Ishihara, 1985)

Figure 21.11 is a summary of damage report during the 1983 Nihonkai-Chubu earthquake in which liquefaction did or did not cause damage at the surface of a level ground (boiling of sand, surface cracks, floating of embedded objects, etc.); slope failure or subsidence of buildings are out of scope. When the thickness of surface unliquefied layer (H_1) was relatively thick when compared with the thickness of liquefied subsoil (H_2), no damage is likely at the surface. Similar studies on other earthquakes resulted in Fig. 21.12 in which curves for a family of surface acceleration are drawn.

Generally speaking, the extent of damage is more substantial when
- F_L is smaller
- The thickness of layer with $F_L < 1$ is greater
- $F_L < 1$ occurs at shallower elevation

These viewpoints are assembled to a single parameter of P_L (Tatsuoka et al. 1980):

$$P_L = \int_0^{20} F(F_L)(10 - 0.5z)\,dz$$

where "z" is the depth in meter, while $F(F_L) = 1 - F_L$ if $F_L \le 1.0$ and $F(F_L) = 0$ if $F_L > 1.0$. Note that the function of depth, 10–0.5z, puts more weights on liquefaction at shallower depth, see Fig. 21.13.

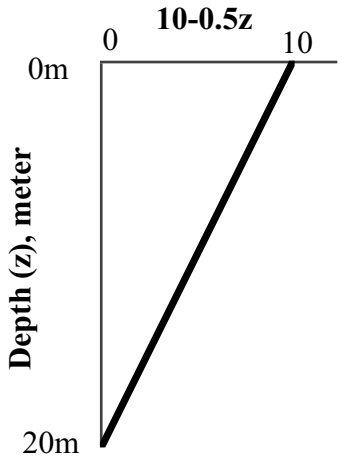

Fig. 21.13 Variation of weight function with depth

Generally, the greater value of P_L occurs when F_L is less than 1.0 at shallow depth over a greater thickness of soil. It is suggested that $P_L > 5$ corresponds to a limited extent of damage, while $P_L > 15$ means a possibility of substantial damage.

There are more correlations between F_L and development of excess pore water pressure (Fig. 23.4) or post-liquefaction subsidence (Fig. 25.22).

21.10 Effects of Frequency on Liquefaction Resistance

Cyclic shear tests on liquefaction resistance of sand are conducted by using either a hydraulic actuator or a pneumatic loader. Although the former can generate cyclic force of higher frequency, which is comparable with a real earthquake loading, its installation is more expensive. The latter employs air pressure and is less expensive, but it is operated at frequency of not more than 0.1 Hz (there is a remarkable development recently to mitigate this technical limitation). Hence, it is frequently asked whether or not this low frequency affects the measured liquefaction resistance of sand.

A pneumatic system may work at a higher frequency as long as the strain of a tested specimen is small. This is because the motion of a loading ram is small and the volume of moving air is small (Fig. 21.14). When the specimen´s deformation is large near the onset of liquefaction, a substantial volume of air has to flow through a tube into a cylinder within a limited time. This is difficult because of viscosity of air and other resistance against air flow.

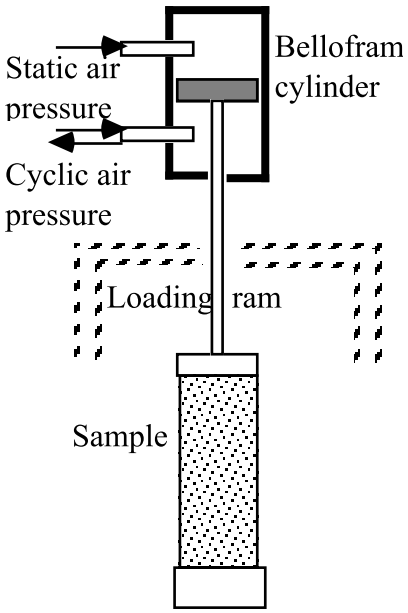

Fig. 21.14 Pneumatic loading system

Figure 21.15 shows the resistance of sand against liquefaction, which was measured by a ring shear apparatus (Yoshimi and Oh-oka, 1975) and cyclic triaxial tests (Wong et al. 1975). In both tests, liquefaction was defined as the first occurrence of 100% rise of excess pore water pressure (initial liquefaction). Despite the range of employed frequency, the difference in the measured liquefaction resistance is negligible. Yasuda and Soga (1984) conducted similar tests, defining liquefaction as the double amplitude of axial strain (peak-to-peak strain) exceeding 5%. Figure 21.16 again shows that loading frequency is not important.

The vertical coordinate in Fig. 21.15 stands for stress ratio of $\tau_{\max}/\sigma'_{\mathrm{vc}}$ in case of ring shear tests (similar to simple shear in mechanism) and $\sigma_{\mathrm{dl}}/\left(2\sigma'_{\mathrm{c}}\right)$ for triaxial tests. The anisotropic stress state (K_0 state) in the former test leads to the reduced stress ratio of $(1+2K_0)/3$ times the latter tests (see C_1 parameter in Sect. 19.4). The discussion in this section concerns sand behavior prior to liquefaction when effective stress does not yet diminish. Hence, there is no rate-dependent (viscous) behavior. In contrast, Sect. 25.17 will discuss post liquefaction behavior in which effective stress has disappeared and rate-dependent behavior becomes more significant.

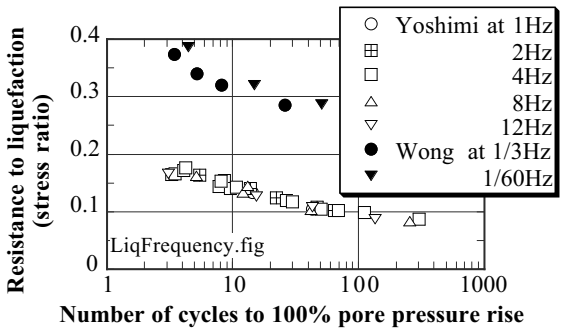

Fig. 21.15 Effects of loading frequency on liquefaction resistance curve of sand (data by Yoshimi and Oh-oka, 1975, and Wong et al. 1975)

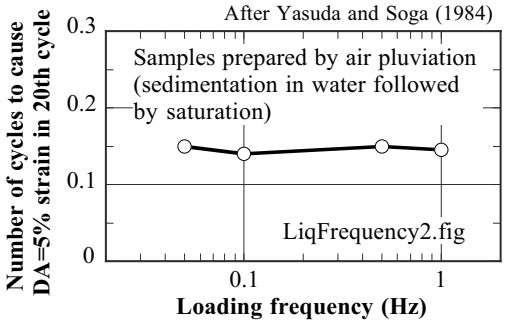

Fig. 21.16 Effects of loading frequency on stress ratio at 20 cycles (Yasuda and Soga, 1984)

21.11 Use of Cone Penetration Tests for Earthquake Geotechnical Survey

Cone penetration test (CPT) is a popular in-situ investigation in which an equipment as in Fig. 21.17 is pushed by a hydraulic mechanism into subsoil at a specified velocity (for example, 1 cm/s); see conceptual Fig. 21.18. This device consists mainly of two parts, which are the cone tip where the tip resistance, q_c, is measured upon penetration and the friction jacket (Begemann, 1953) where skin friction, f_s, is recorded independent of the tip resistance. The order of penetration of these two parts is illustrated in Fig. 21.19. Firstly, the cone tip is pushed to measure the tip resistance, and then the friction jacket goes down to record the skin friction.

A portable cone penetrometer (Fig. 21.20) is a useful tool for field investigation as well. Its penetration capacity is, however, limited by human power and hence is applicable only to soft clay or similar soil. Its penetration in sandy ground is difficult.

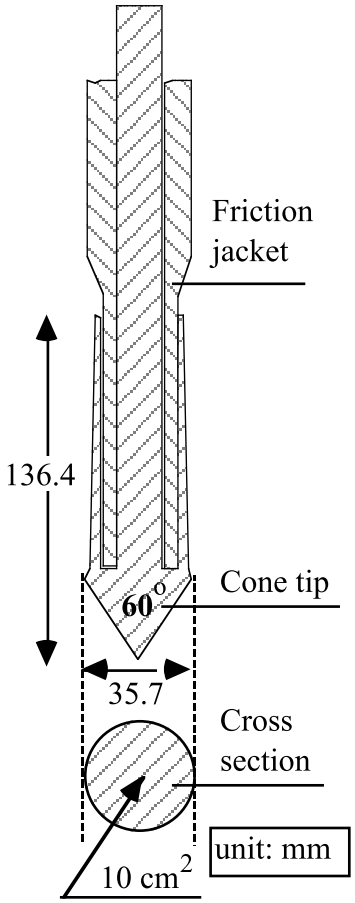

Fig. 21.17 CPT equipment

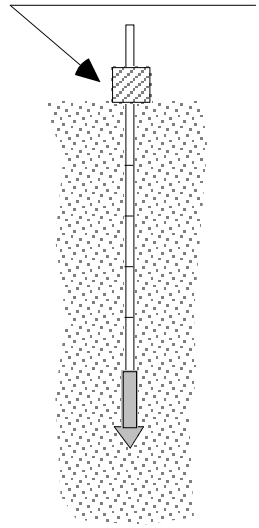

Fig. 21.18 Penetration of CPT device into subsoil

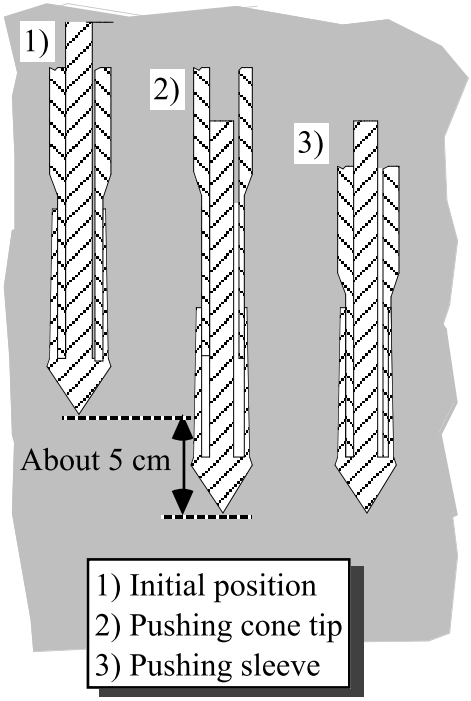

Fig. 21.19 Detailed procedure of CPT penetration

Fig. 21.20 Portable cone penetrometer for soft clay (photo by S. Nishimura)

CPT has been used widely to assess the rigidity of soil, bearing capacity of foundation, and other subsoil properties by using their empirical correlations with cone tip resistance.

CPT has such advantages as

1. No need for drilling a bore hole
2. Being therefore economical and time-efficient
3. Data being less subject to personal difference

To make use of these advantages, there are recent technical developments such as

– Electric cone that records pore water pressure during penetration
– Seismic cone which measures S-wave propagation time and determines V_s (Campanella and Davies, 1994).

One shortcoming of CPT may be that no soil sample is collected, whether disturbed or undisturbed. Therefore, it is not easy to determine the type of soil, particle size, and plasticity. Although SPT-*N* value (standard penetration tests; Sects. 1.12, 8.4, 21.1) has the same problem, SPT allows eye inspection of collected disturbed samples (Fig. 1.37), while CPT does not. SPT further allows tests on physical properties such as gradation and plasticity index.

Attempts have been made to overcome this problem of CPT by developing empirical correlation between soil type and the ratio between skin friction, f_s, and tip resistance, q_c. For example, Begemann (1965) proposed a design chart in which a combination of cone tip resistance and the ratio of friction to tip resistance is employed for soil classification. For the same purpose, Robertson (1990) proposed to use the normalized cone tip resistance, $\left(q_c - \sigma_{vo}\right)/\sigma'_{vo}$ and friction, $f_s/\left(q_c - \sigma_{vo}\right)$, where σ_{vo} and σ'_{vo} stand for the total and effective vertical stress at respective depth. In their idea, greater (normalized) tip resistance and lower (normalized) friction means sand and gravel, and in contrast , lower tip resistance and higher friction come from clayey soils.

Shibata and Teparaksa (1988) collected information on CPT tip resistance, q_c, from sites with and without liquefaction. Since the tip resistance is affected by the in-situ effective vertical stress (σ'_{vo}), it was corrected by

$$q_{c1} = \left(\frac{0.17}{\sigma'_{vo} + 0.07}\right) q_c, \qquad (21.9)$$

in which the unit of stress is MPa. Thus, the normalized cone resistance, q_{c1}, at the effective stress of 0.1 MPa (1 kgf/cm^2) was obtained. Since fine grains in soil affect the cone resistance and liquefaction resistance of soil, the normalized cone resistance was further modified by introducing a factor of C_2

$C_2 = 1$ when the mean grain size (D_{50}, mm) is greater than 0.25 mm
$C_2 = D_{50}/0.25$ when D_{50}<0.25 mm.

Thus, the liquefaction potential was judged by using q_{c1}/C_2.

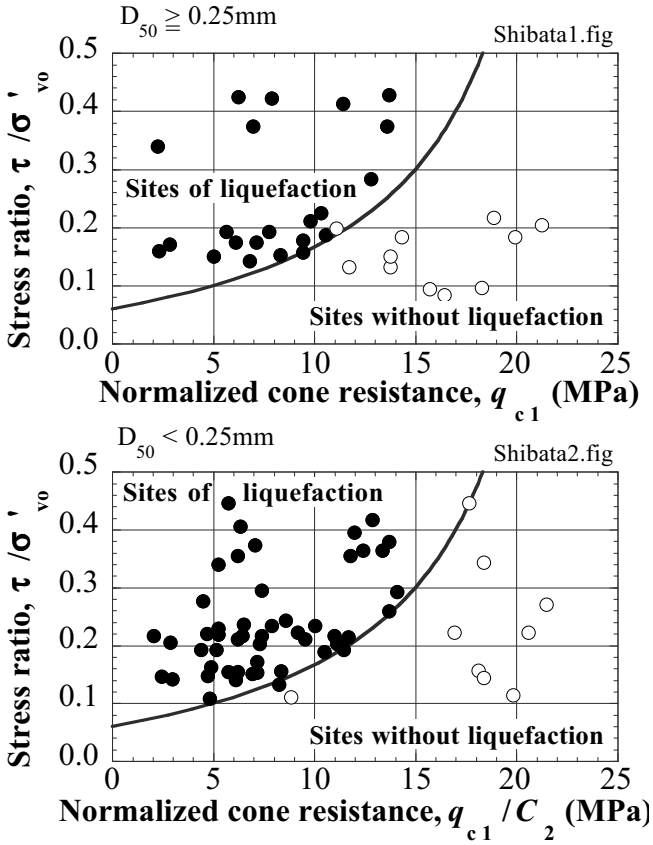

Fig. 21.21 Relationship between normalized cone tip resistance and stress ratio during earthquakes (after Shibata and Teparaksa, 1988)

Figure 21.21 compares this new cone tip parameter and the field stress ratio, τ/σ'_{vo}, which was assessed by using recorded motion during earthquakes. It is shown therein that there is a clear boundary between cases with and without liquefaction. Shibata and Teparaksa (1988) expressed this boundary curve by

$$\frac{q_{c1}}{C_2} = 5 + 20\left(\frac{\dfrac{\tau}{\sigma'_{vo}} - 0.1}{\dfrac{\tau}{\sigma'_{vo}} + 0.1}\right). \qquad (21.10)$$

Note that the more recent knowledge of fines content states that cohesive fines increases the liquefaction resistance of soils (Sect. 20.4), while cohesionless (non-plastic) fines does not (Sect. 20.5).

Robertson (1990) further proposed to classify soil type by using pore water pressure, which is measured beside the cone tip; generally, higher pore pressure implies finer soils.

Since CPT investigation is quick and economical, it is meaningful to apply this technology to detailed field investigation on liquefaction potential. "Detailed" means that the number of tests per unit area is so large that complicated geographical and geological conditions are accurately understood. In this respect, Robertson and Wride (1998) proposed to determine liquefaction resistance based on cone resistance. Note, however, that their data was based on conversion from SPT-N to CPT, which relied on many empirical knowledge of correlation.

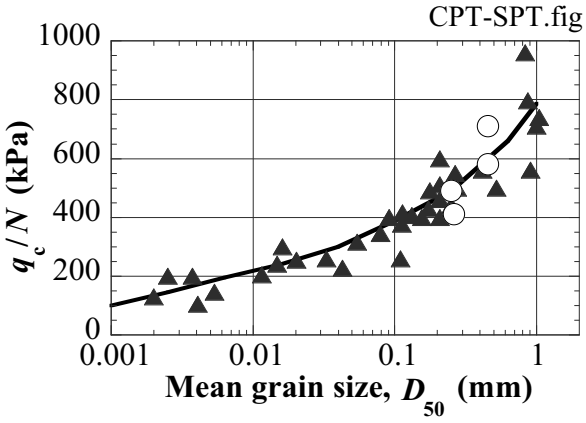

Fig. 21.22 Empirical correlation between CPT/SPT ratio and mean grain size (drawn after Robertson et al., 1983)

Robertson et al. (1983) collected data of q_c / N from many literatures. Since this ratio had a wide range of variation, they further studied the correlation between q_c / N and the grain size. Figure 21.22 reveals a reasonable correlation which made it possible to convert the existing SPT-N correlation to a CPT correlation.

Noteworthy is that the cone tip resistance, q_c, is normalized in terms of the effective vertical stress, σ'_{vo}. This implies that the measured q_c leads to an overestimation of the sand density due to increased shear resistance under higher effective stress. The normalized cone resistance, q_{C1N}, is given by

$$q_{C1N} = \left(\frac{q_c}{P_a}\right)\left(\frac{P_a}{\sigma'_{vo}}\right)^n, \qquad (21.11)$$

in which P_a designates the atmospheric pressure (= 98 kPa) and n = 0.5 typically.

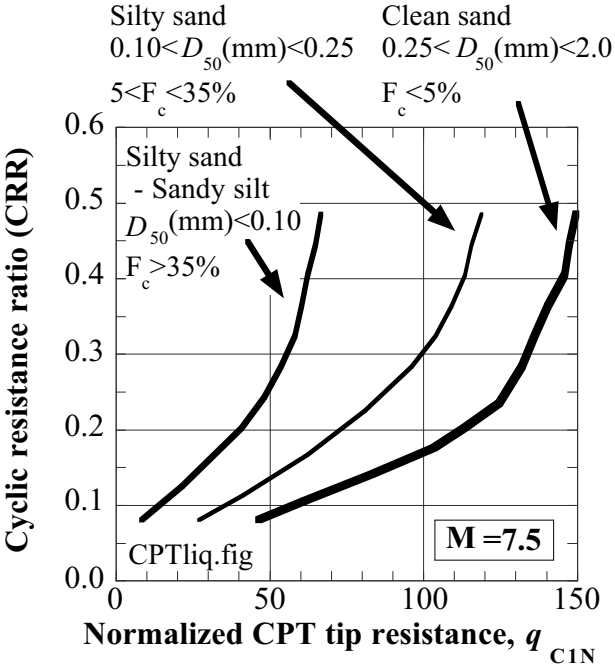

Fig. 21.23 Resistance of soil against liquefaction as assessed from cone penetration resistance (after Robertson and Wride, 1998)

There are many data of SPT-N at sites with and without liquefaction (Fig. 21.2). Those SPT data were converted to CPT as mentioned above and the curves in Fig. 21.23 was obtained. In this diagram, liquefaction resistance or stress ratio CRR for soils of different fines content (F_c) are illustrated as functions of the normalized cone resistance.

It should be noted that CPT cannot directly identify the soil type or fines content (F_c) in Fig. 21.21. Soil types have to be identified separately. The fines in this figure seems to mean cohesive fine soils and therefore the cohesionless fine soil (for example, highly liquefiable tailing material in Sect. 20.5) is out of scope.

21.12 Use of S-Wave Velocity for Liquefaction Investigation

Denser sand has greater resistance against liquefaction. Denser sand has greater shear modulus, G_{max}, and S wave velocity, $V_s = \sqrt{G_{max}/\rho}$. Therefore, it is expected that V_s is a good index of liquefaction resistance of in-situ soils. This idea becomes more attractive because V_s can be economically measured by a seismic cone (Campanela and Davis, 1994) or surface wave monitoring (SASW in Sect. 8.11). Studies in this direction were conducted by Stokoe and Nazarian (1985) as well as Andrus and Stokoe (1996, 2000).

Robertson et al. (1992) collected V_s values from cases of several earthquakes. The boundary of liquefied and unliquefied sites results in Fig. 21.24. In this figure, the measured V_s value was corrected for the effect of overburden pressure by

$$V_{S1} = V_s\left(\frac{P_a}{\sigma'_{vo}}\right)^{0.25}, \qquad (21.12)$$

where P_a stands for the atmospheric pressure.

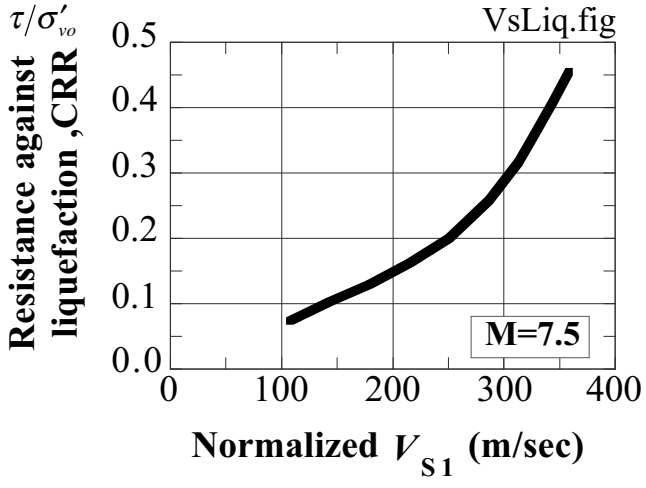

Fig. 21.24 Correlation between liquefaction resistance and S wave velocity (after Robertson et al., 1992)

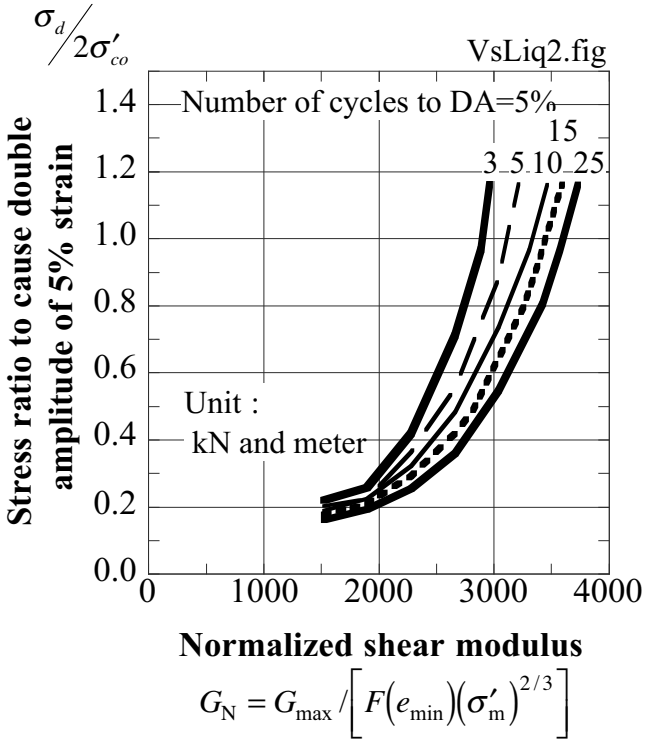

Fig. 21.25 Experimental relationship between normalized shear modulus and resistance against liquefaction (after Tokimatsu and Uchida, 1990)

Tokimatsu and Uchida (1990) demonstrated the use of V_s as what follows.

1. S wave velocity, V_s, is converted to shear modulus at small strain amplitude, $G_{max} = \rho V_S^2$.
2. G_{max} is normalized in terms of mean effective stress, σ'_m, and the minimum void ratio, e_{min}

$$G_N = G_{max} / \left[F(e_{min})(\sigma'_m)^n \right], \quad (21.13)$$

where n is between 1/3 and 2/3, and the F function is defined by

$$F(e_{min}) = \frac{(2.17 - e_{min})^2}{1 + e_{min}}. \qquad (21.14)$$

The mean effective stress is determined by using the effective vertical stress, σ'_{vo}, and an assessed value of earth pressure coefficient at rest (K_0)

$$\sigma'_m = \frac{1+2K_0}{3}\sigma'_{vo}. \qquad (21.15)$$

3. Figure 21.25 illustrates a summary of experimental relationships between G_N and stress ratio (resistance to liquefaction), which is needed to trigger liquefaction after a variety of number of cycles. The number of cycles in design earthquakes can be determined by using Table 19.1. The minimum void ratio is evaluated without collecting soil samples (V_s survey) by using a Sakai-Yasuda (1977) empirical diagram (Fig. 21.26).
4. The field resistance against liquefaction is determined by

$$\frac{\tau}{\sigma'_{vo}} = \frac{1+2K_0}{3}\frac{\sigma_d}{2\sigma'_{co}}. \qquad (21.16)$$

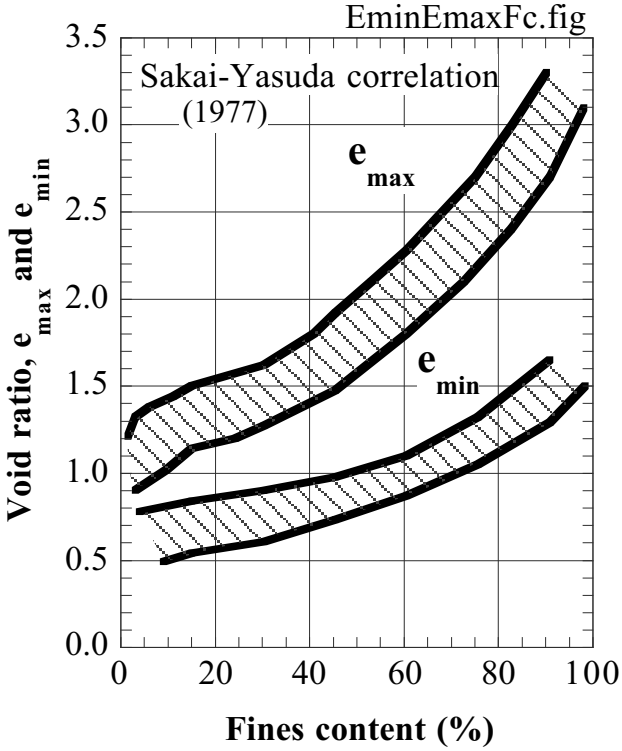

Fig. 21.26 Sakai-Yasuda relationship between fines content and minimum void ratio of sand

Noteworthy is that field investigation of V_s cannot identify directly the type of soil. Liquefiable sand and unliquefiable clay may have the same V_s but they cannot be discriminated without collecting soil samples. In this situation, it is advisable to combine V_s survey with other kind of soil investigation that can identify types of soil. For example, SPT soil profiles are interpolated by more economical V_s investigations (Sect. 22.5).

List of References in Chapter 21

Andrus, R.D. and Stokoe, II., K.H. (1996) Preliminary guidelines for liquefaction assessment using shear wave velocity, UJNR 28th Joint Meting of United States-Japan Panel on Wind and Seismic Effects, Gaithersburg, Maryland:

Andrus, R.D. and Stokoe II, K.H. (2000) Liquefaction resistance of soils from shear-wave velocity, Begemann, H.K.S.P. (1953) Improved method of determining resistance to adhesion by sounding through a loose sleeve placed behind the cone, Proc. 3rd Int. Conf. Soil Mech. Found. Eng., Vol. 1, pp. 213–217.

Begemann, H.K.S.P. (1965) The friction jacket cone as an aid in determining the soil profile, Proc. 6th Int. Conf. Soil Mech. Found. Eng., Vol. 1, pp. 17–20.

Campanella, R.G. and Davies, M.P. (1994) The seismic piezocone: a practical site investigation tool, Geophysical Characterization of Sites, Ed. R.D. Woods, Publication of Technical Committee No. 10 of Int. Soc. Soil Mech. Found. Eng., publ. Oxford & IBH Publishers, pp. 49–55.

Highway Bridge Design Code (道路橋示方書) (1990) Japan Road Association, Part Ⅴ, Seismic Design (this has been updated periodically later).

Ishihara, K. (1985) Stability of natural deposits during earthquakes, Theme Lecture at 11th ICSMFE (Int. Conf. Soil Mech. Found. Eng.), San Francisco, Vol. 1, pp. 321–376.

Kishida, H. (1966) Damage to reinforced concrete buildings in Niigata City with special reference to foundation engineering, Soil. Found., Vol. 6, No. 2, pp. 71–88.

Koizumi, Y. (1966) Change in density of sand subsoil caused by the Niigata Earthquake, Soil. Found., Vol. 6, No. 2, pp. 38–44.

Meyerhof, G.G. (1957) Discussion of Session 1, Proc. 4th Int. Conf. Soil Mech. Found. Eng., Vol. 3, p. 110.

Robertson, P.K. (1990) Soil classification using the cone penetration test, Can. Geotech. J., Vol. 27, pp. 151–158.

Robertson, P.K., Campanella, R.G. and Wightman, A. (1983) SPT-CPT correlations, J. Geotech. Eng., ASCE, Vol. 109, GT11, pp. 1449–1459.

Robertson, P.K., Woeller, D.J. and Finn, W.D.L. (1992) Seismic cone penetration test for evaluating liquefaction potential under cyclic loading, Can. Geotech. J., Vol. 29, pp. 686–695.

Robertson, P.K. and Wride, C.E. (1998) Evaluating cyclic liquefaction potential using the cone penetration test, Can. Geotech. J., Vol. 35, pp. 442–459.

Sakai, Y. and Yasuda, S. (1977) Liquefaction characteristics of undisturbed sandy soils, Proc. 12th Annual Conf. of JSSMFE, pp. 389–392 (in Japanese).

Seed, H.B. (1987) Design problems in soil liquefaction, J. Geotech. Eng., Vol. 113, No. 8, pp. 827–845.

Seed, H.B. and Idriss, I.M. (1982) Ground motions and soil liquefaction during earthquakes, Earthq. Eng. Res. Inst., ISBN 0-943198-24-0, p. 107.

Seed, H.B., Tokimatsu, K., Harder, L.F. and Chung, R.M. (1985) Influence of SPT procedures in soil liquefaction resistance evaluations, Proc. ASCE, Vol. 111, GT12, pp. 1425–1445.

Shibata, T. and Teparaksa, W. (1988) Evaluation of liquefaction potential of soils using cone penetration tests, Soil. Found., Vol. 28, No. 2, pp. 49–60.

Stokoe, K.H. and Nazarian, S. (1985) Use of Rayleigh waves in liquefaction studies, Measurement and use of shear wave velocity, Ed. R.D. Woods, ASCE, pp. 1–17.

Tatsuoka, F., Iwasaki, T., Tokida, K., Yasuda, S., Hirose, M., Imai, T. and Kon-no, M. (1980) Standard penetration tests and soil liquefaction potential evaluation, Soil. Found., Vol. 20, No. 4, 95–111.

Tokimatsu, K. and Uchida, A. (1990) Correlation between liquefaction resistance and shear wave velocity, Soil. Found., Vol. 30, No. 2, pp. 33–42.

Wong, R.T., Seed, H.B. and Chan, C.K. (1975) Cyclic loading liquefaction of gravelly soils, Proc. ASCE, Vol. 101, GT6, pp. 571–583.

Yasuda, S. and Soga, M. (1984) Effect of frequency on undrained strength of sands, Proc. 19th Nat. Conf. Soil Mech. Found. Eng, pp. 549–550 (in Japanese).

Yoshimi, Y. and Oh-oka, H. (1975) Influence of degree of shear stress reversal on the liquefaction potential of saturated sand, Soil. Found., Vol. 15, No. 3, pp. 27–40.